Journal of Alloys and Compounds 516 (2012) 65–72

Contents lists available at SciVerse ScienceDirect

Journal of Alloys and Compounds

journal homepage: www.elsevier.com/locate/jallcom

The crystal and electronic band structure of the diamond-like semiconductor Ag_2ZnSiS_4

Carl D. Brunetta, Balamurugan Karuppannan, Kimberly A. Rosmus, Jennifer A. Aitken*

Department of Chemistry and Biochemistry, Duquesne University, 600 Forbes Avenue, Pittsburgh, PA 15282, USA

ARTICLE INFO

Article history:
Received 30 September 2011
Received in revised form
23 November 2011
Accepted 25 November 2011
Available online 6 December 2011

Keywords:
Diamond-like semiconductor
Band structure
Density of states
Wien2k
Metal sulfide

ABSTRACT

Single crystals of the new diamond-like semiconductor Ag_2ZnSiS_4 have been synthesized using high-temperature, solid state synthesis at 800 °C. The compound crystallizes in the monoclinic, non-centrosymmetric space group *Pn* with $a = 6.4052(1)$ Å, $b = 6.5484(1)$ Å, $c = 7.9340(1)$ Å, $\beta = 90.455(1)°$ and $R1$ (for all data) = 2.42%. The electronic band structure and density of states were calculated using density functional theory (DFT) and the full potential linearized augmented plane wave (LAPW) method within the Wien2k program suite. The calculated band structure suggests that Ag_2ZnSiS_4 is a direct band gap semiconductor with a calculated band gap of 1.88 eV at the Γ-point. The calculated density of states of Ag_2ZnSiS_4 is compared with that of $AgGaS_2$. The band gap of Ag_2ZnSiS_4 was also determined experimentally as 3.28 eV via optical diffuse reflectance spectroscopy.

1. Introduction

Over the past few years, multi-cation diamond-like semiconductors (DLSs) have received increased attention for their promising physical properties. A work by Shi et al. showed that $Cu_2Sn_{1-x}In_xSe_3$ possess an impressive thermoelectric figure of merit, ZT, of 1.14 at 850 K [1] indicating its potential use in thermoelectric applications. A recent work on the compound $Cu_2ZnSnSe_4$ (CZTSe) has shown that the substitution of In for Sn increases ZT from 0.28 in the native compound to 0.95 in the 10% In substituted phase [2]. Another work by Steinhagen et al. has demonstrated that Cu_2ZnSnS_4 (CZTS) can be synthesized as nanocrystals in the kesterite structure which can be used as a cheaper route for the production of photovoltaic devices [3]. Furthermore in 2009, Lekse et al. reported that Li_2CdSnS_4 exhibits a second harmonic generation (SHG) response 100× that of α-quartz and is phase matchable [4]. They suggest that quaternary DLSs with larger band gaps should possess increased laser damage thresholds as compared to the commercially available ternary DLSs that are currently used in nonlinear optical devices [5,6]. While these recent studies focus on the technologically useful properties of multication DLSs, one of the key elements in understanding these materials as a class is the correlation between these desirable attributes and crystal structure.

The above compounds are all diamond-like, i.e. they have a structure that resembles either cubic or hexagonal diamond [7,8] as shown in, Fig. 1. These materials follow a set of guidelines that includes, (i) each atom must have an average valence electron concentration of 4, (ii) the average concentration of valence electrons for each anion must be 8 [7,8], (iii) each atom must have a tetrahedral coordination, and (iv) the octet of each anion must be satisfied by its nearest neighbors [7–9]. These guidelines can be used not only to classify the known compounds but also to predict new compounds. Furthermore, combining these rules with an understanding of how the structure of these materials relates to the physical properties could prove useful in predicting properties of yet to be discovered materials.

This work presents the crystal structure, electronic band structure, and density of states (DOS) of the DLS Ag_2ZnSiS_4 as well as the experimentally determined band gap. Ag_2ZnSiS_4 is a quaternary DLS of the formula I_2-II-IV-VI_4, which can be derived from that of the I-III-VI_2 family, with $AgGaS_2$ being its closest ternary relative. The structure of Ag_2ZnSiS_4 can be obtained from $AgGaS_2$ by replacing every two Ga atoms in a doubled structure of $AgGaS_2$ with one Zn and one Si in an ordered fashion (see Fig. 1). Therefore the band structure and DOS of Ag_2ZnSiS_4 are compared with that of $AgGaS_2$ computed using the same method [10].

* Corresponding author. Tel.: +1 412 369 1670; fax: +1 412 369 5683.
E-mail address: aitkenj@duq.edu (J.A. Aitken).

0925-8388/$ – see front matter © 2011 Elsevier B.V. All rights reserved.
doi:10.1016/j.jallcom.2011.11.133

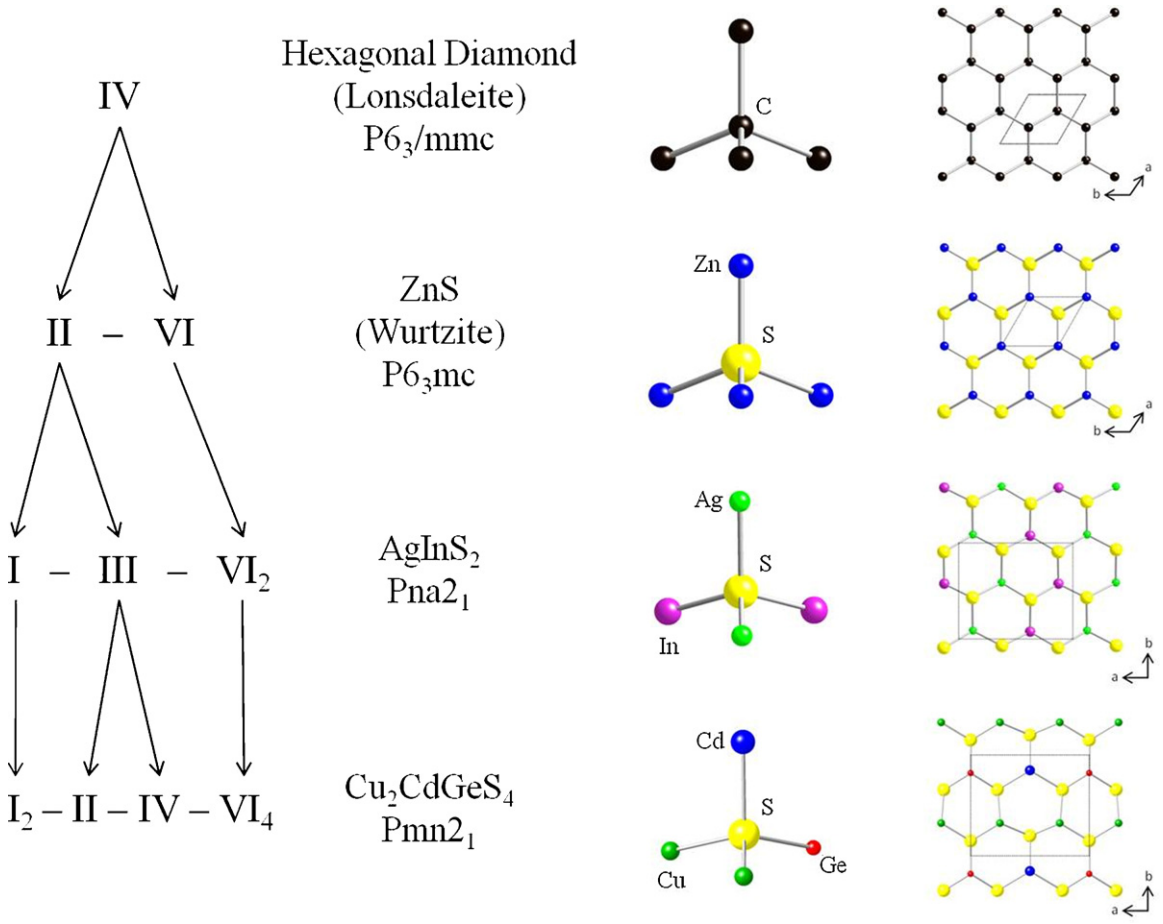

Fig. 1. Structural progression of the hexagonal family of DLSs, showing the most common space groups at each level.

2. Experimental

2.1. Reagents

Chemicals used in this work were utilized as obtained unless otherwise noted: (1) silver powder, ~325 mesh, 99.99%, Cerac Milwaukee, WI; (2) zinc powder, 99.999%, Strem, Newburyport, MA; (3) silicon powder, 99.999%, Strem, Newburyport, MA; (4) sulfur powder, sublimed, 99.5%, Fisher Scientific, Pittsburgh, PA.

2.2. Synthetic procedure, Ag_2ZnSiS_4

Single crystals of Ag_2ZnSiS_4 were produced by weighing 4 mmol of Ag, 2 mmol of Zn, 2 mmol of Si, and 8 mmol of S in an argon-filled glove box. These reagents were combined using an agate mortar and pestle until the sample appeared homogeneous (~20 min). The mixed powder was then transferred to a graphite crucible which was placed into a 12 mm O.D. fused-silica tube. The tube was flame-sealed under a vacuum of approximately 10^{-3} mbar and placed in a programmable muffle furnace. The reactants were heated to 800 °C over 12 h and held at that temperature for 96 h. After which the sample was slow-cooled to 500 °C at 5 °C/h (60 h) and then allowed to cool radiatively to ambient temperature.

The product was a gray colored ingot with colorless needle-like crystals slightly tinted green protruding from the surface. Energy dispersive spectroscopy (EDS) showed the presence of all four elements in the translucent crystals.

2.3. Physical property measurements

2.3.1. Scanning electron microscopy and energy dispersive spectroscopy (SEM/EDS)

SEM/EDS was performed on a Hitachi S-3400N scanning electron microscope equipped with a Bruker Quantax model 400 energy dispersive spectrometer using an XFlash® 5010 EDS detector with a 129 eV resolution. Samples were mounted on double-sided carbon tape affixed to an aluminum specimen holder. Images were taken at a working distance of 10 mm with an accelerating voltage of 15 kV. EDS spectra were also collected under the same conditions for 2 min live time.

2.3.2. Single-crystal X-ray diffraction data collection and reduction

A Bruker SMART Apex 2 CCD single crystal X-ray diffractometer employing graphite monochromatized molybdenum K_α radiation with a wavelength of 0.7107 Å and operating with a tube power of 50 kV and 30 mA was used to collect the data for 40 s/frame at ambient temperature. A total of 4283 measured reflections were collected with 1456 unique. The program SAINT was used to integrate the data and SADABS was employed to perform the absorption correction [11,12]. XPREP was used for space group determination and to create files for SHELXTL. Based on systematic absences, two space groups were initially considered, *Pn* and *P2/n*. The space group *Pn* (No. 7) was selected because all DLSs are noncentrosymmetric due to all of the tetrahedra pointing in the same direction along a crystallographic axis.

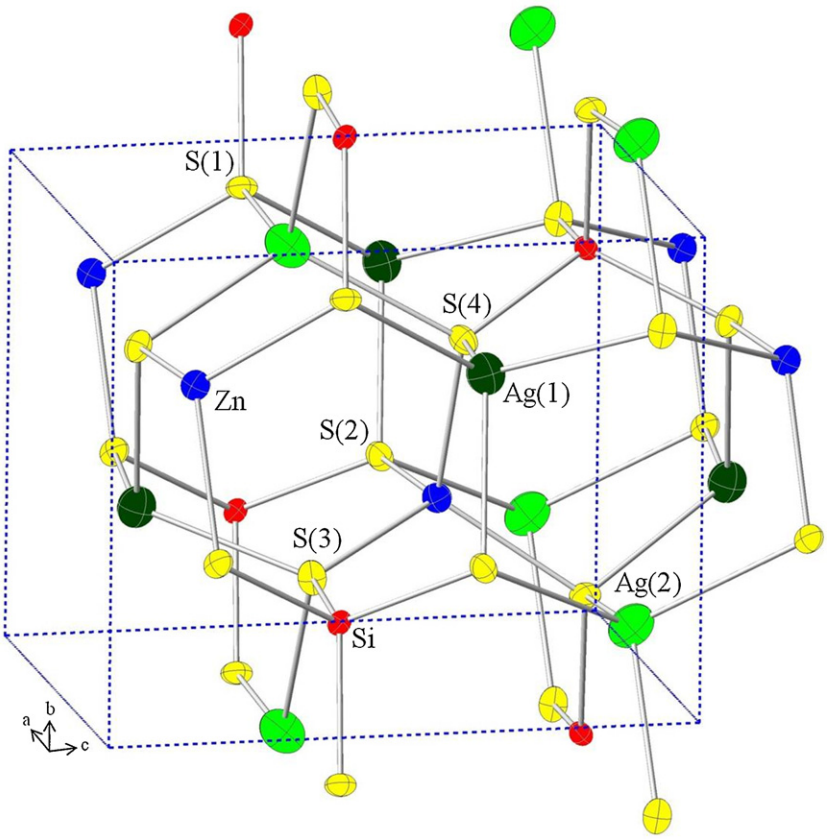

Fig. 2. Unit cell of Ag_2ZnSiS_4 using thermal ellipsoids with 50% probability.

2.3.3. Single crystal structure solution and refinement

Using the SHELXTL-PC [13] software package, the structure was solved and refined in the noncentrosymmetric space group *Pn*, Fig. 2. Eight atoms were located on general positions; 2 Ag sites, 1 Zn site, 1 Si site and 4 S sites. The structure was refined with an *R*1 (all data) of 0.0210. Other crystallographic and experimental details are reported in Table 1. Fractional atomic coordinates and equivalent isotropic displacement parameters are given in Table 2 while refined bond distances and angles are shown in Table 3. The program CrystalMaker® [14] was used to generate the crystal structure figures.

2.3.4. X-ray powder diffraction (XRPD)

X-ray powder diffraction studies were performed on a Panalytical X'Pert Pro MPD powder X-ray diffractometer using copper K_α radiation with a wavelength of 1.541871 Å and operating with a tube power of 45 kV 40 mA. Data were collected from 5° to 145° 2θ with a step size of 0.0083556° and scan rate of 0.010644°/s. The incident beam optics were comprised of a 0.02 rad soller slit, a divergent slit of 1/4° and an anti-scatter slit of 1/2°; whereas, the diffracted beam optics were comprised of a 0.02 rad soller slit and an anti-scatter slit of 1/4°. The samples were prepared for analysis using a top fill method where the sample powder is added from bottom to top of a sample holder and spread out gently using a razor blade to minimize preferred orientation. Phase identification of crystalline components was carried out using the X'Pert HighScore Plus software package [15] and the International Center for Diffraction Data (ICDD) database.

2.3.5. Diffuse reflectance UV/Vis/NIR spectroscopy

Diffuse reflectance UV/Vis/NIR spectroscopy was performed using a Varian Cary 5000 spectrometer equipped with a Harrick Praying Mantis diffuse reflectance accessory. The sample was ground, placed in the sample cup and compared to a similarly prepared 100% reflectance standard, $BaSO_4$. Data were collected from 2500 to 200 nm at a scan rate of 600 nm/min. The collected percent

Table 1
Crystallographic data and experimental details for Ag_2ZnSiS_4.

Empirical formula	Ag_2ZnSiS_4
Size	0.025 mm × 0.032 mm × 0.237 mm
Color	Colorless
Habit	Needle
Formula weight	437.44 g mol^{-1}
Temperature	296(2) K
Wavelength of X-ray	0.71073 Å
Space group	*Pn*
Unit cell dimensions	a = 6.4052(1) Å
	b = 6.5484(1) Å
	c = 7.9340(1) Å
	$\alpha = \gamma = 90°$
	β = 90.455(1)°
Volume	332.772(8) Å^3
Z	2
Calculated density	4.366 Mg m^{-3}
Flack parameter	0.04(1)
F(000)	404
Reflections collected/unique	4283/1456
Data/restraints/parameters	1456/2/75
Completeness to theta = 27.11°	100.0%
Goodness of fit	1.272
Final *R* indices [$I > 2$sigma(I)]	$R1$ = 0.0197, wR_2 = 0.0402
R indices (all data)	$R1$ = 0.0210, wR_2 = 0.0411

Refinement of F^2 was made against all reflections. $R1 = (\Sigma\,||F_o| - |F_c||)/\Sigma|F_o|$, $wR_2 = \sqrt{(\Sigma[w(F_o^2 - F_c^2)])/\Sigma[w(F_o^2)]}$, $w = 1/(\sigma^2(F_o^2) + (aF_o)^2 + bP)$, $P = [2F_c^2 + Max(F_o^2, 0)]/3$.

Table 2
Fractional atomic coordinates and equivalent isotropic displacement parameters, U_{iso} (Å^2 × 10^3) for Ag_2ZnSiS_4.

Site	x	y	z	$U_{(eq)}$[a]
Ag(1)	0.23428 (4)	0.31806 (5)	0.32726 (3)	29 (1)
Ag(2)	0.71991 (6)	0.15354 (4)	0.57873 (5)	33 (1)
Si(1)	0.7199 (3)	0.1844 (1)	0.0732 (2)	11 (1)
Zn(1)	0.22232 (7)	0.31373 (7)	0.82066 (5)	16 (1)
S(1)	0.1161 (1)	0.1248 (1)	0.5868 (1)	14 (1)
S(2)	0.5879 (1)	0.3163 (1)	0.8534 (1)	15 (1)
S(3)	0.0504 (1)	0.2008 (1)	0.0614 (1)	16 (1)
S(4)	0.6239 (1)	0.3398 (1)	0.2966 (1)	14 (1)

[a] $U_{(eq)}$ is defined as 1/3 the trace of the orthogonal tensor U_{ij}.

reflectance was converted to absorbance using the Kubelka–Munk equation [16] and wavelength was converted to eV.

2.3.6. Electronic structure calculations

Density functional theory (DFT) calculations were performed using the solid state electronic structure package, Wien2k (version 11.1) [17]. Wien2k uses a hybrid full potential linear augmented plane wave (LAPW) and augmented plane wave + local orbitals (APW + lo) schemes for solving the Kohn-Sham (KS) equations of the total energy of crystalline solids within DFT. In the LAPW method, the unit cell of a crystal is partitioned into non-overlapping atomic spheres and interstitial regions. The basis functions are constructed using the muffin-tin approximation (MTA), in which spherically symmetric potential within the atomic spheres and constant potential outside the spheres are assumed. The electronic states are classified as core, semi-core and valence states. The core states are completely confined within the atomic sphere while the semi-core states are high-lying core states that are not completely confined within the atomic sphere. The valence states are (partly) delocalized [18]. The APW + lo method increases the computation speed while its results are comparable in accuracy with that of LAPW method [19]. The results presented here are based on the calculations using APW + lo methods of Wien2k.

The refined structure of Ag_2ZnSiS_4 (obtained in the single crystal XRD studies in this work) and the structure of $AgGaS_2$ given by Laksari et al. [10] were used in the DFT calculations. For the case of Ag_2ZnSiS_4, the Ag, Zn, Si and S atoms with electronic configurations, [Kr] $4d^{10}$ $5s^1$, [Ar] $3d^{10}$ $4s^2$, [Ne] $3s^2$ $3p^2$ and [Ne] $3s^2$ $3p^4$ were modeled to have MT spheres of radii (R_{MT}) 2.48, 2.29, 1.97 and 1.97 bohr respectively. On the other hand, following Laksari et al. [10], the MT spheres of radii 2.2, 2.0 and 1.8 for Ag, Ga ([Ar] $3d^{10}$ $4s^2$ $4p^1$) and S respectively are taken for the case of $AgGaS_2$. The Perdew–Burke–Ernzerhof generalized gradient approximation (PBE-GGA) was used in the calculation for treating the exchange and correlation effects. The calculations for the case of $AgGaS_2$ were also carried out using the local spin density approximation (LSDA) and their results are presented in Supplementary Material. These were performed in order to more directly compare to calculations already found in the literature [10,20]. The product of minimum of R_{MT} and K_{max} (RK_{max}) was set to be 7.0 for the case Ag_2ZnSiS_4 and 8.0 for $AgGaS_2$. For both the compounds: (i) the self consistent calculations were considered to be converged only if the energy change is less than 0.1 mRy/unit cell, (ii) the k-mesh was generated using a total of 1000 *k*-points in the whole Brillouin zone (BZ), (iii) the high symmetry points taken for plotting the band structure within the irreducible Brillouin zone (IBZ) are in an automatic (arbitrary) path based on the template files of Wien2k.

Table 3
Selected bond distances (Å) and angles (°) for Ag_2ZnSiS_4.

Bond	Distance (Å)	Bond	Angle (°)
Ag(1)—S(1)	2.537(1)	S(1)—Ag(1)—S(2)	106.65(3)
Ag(1)—S(2)	2.5802(8)	S(1)—Ag(1)—S(3)	112.69(3)
Ag(1)—S(3)	2.527(1)	S(1)—Ag(1)—S(4)	114.18(3)
Ag(1)—S(4)	2.513(1)	S(2)—Ag(1)—S(3)	100.47(3)
		S(2)—Ag(1)—S(4)	108.48(3)
		S(3)—Ag(1)—S(4)	113.14(4)
Ag(2)—S(1)	2.545(1)	S(1)—Ag(2)—S(2)	110.08(4)
Ag(2)—S(2)	2.575(1)	S(1)—Ag(2)—S(3)	110.86(3)
Ag(2)—S(3)	2.565(1)	S(1)—Ag(2)—S(4)	106.46(4)
Ag(2)—S(4)	2.618(1)	S(2)—Ag(2)—S(3)	106.14(4)
		S(2)—Ag(2)—S(4)	117.02(3)
		S(3)—Ag(2)—S(4)	106.21(4)
Zn(1)—S(1)	2.327(1)	S(1)—Zn(1)—S(2)	112.09(5)
Zn(1)—S(2)	2.354(1)	S(1)—Zn(1)—S(3)	110.33(4)
Zn(1)—S(3)	2.333(1)	S(1)—Zn(1)—S(4)	111.71(4)
Zn(1)—S(4)	2.3623(9)	S(2)—Zn(1)—S(3)	112.81(5)
		S(2)—Zn(1)—S(4)	105.46(4)
		S(3)—Zn(1)—S(4)	104.08(5)
Si(1)—S(1)	2.135(1)	S(1)—Si(1)—S(2)	107.84(9)
Si(1)—S(2)	2.116(2)	S(1)—Si(1)—S(3)	111.18(8)
Si(1)—S(3)	2.122(3)	S(1)—Si(1)—S(4)	108.5(1)
Si(1)—S(4)	2.138(2)	S(2)—Si(1)—S(3)	109.6(1)
		S(2)—Si(1)—S(4)	111.91(8)
		S(3)—Si(1)—S(4)	107.8(1)

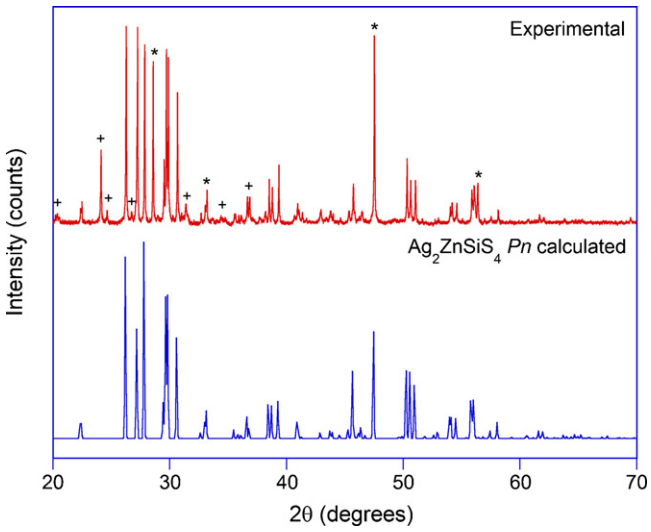

Fig. 3. X-ray powder diffraction pattern of the ground ingot (top) compared to the calculated pattern of Ag_2ZnSiS_4 (bottom). Peaks indexed to the impurity phases ZnS (*) and Ag_2SiS_3 (+) are also indicated.

3. Results and discussion

3.1. Morphology and composition

Reactions to prepare Ag_2ZnSiS_4 produced a gray ingot with colorless crystals with what appeared to have a very slight green tint on the surface. When the ingot was broken, cavities were observed within the ingot where more crystals were found. EDS analysis of the gray ingot showed regions of Ag_2ZnSiS_4, ZnS and an Ag–Si–S phase. X-ray powder diffraction of the ground ingot (Fig. 3) shows the presence of the quaternary phase Ag_2ZnSiS_4. The powder pattern also shows the presence of two unwanted phases, ZnS and Ag_2SiS_3, in the bulk sample. EDS spectra of the crystals show the presence of all four elements (Fig. 4) in the measured ratio of $Ag_{1.97}Zn_1Si_{1.15}S_{4.13}$ in agreement with the crystal structure. A higher concentration of Zn was detected within the crystals than on the surface which is due to a possible surface coating of an impurity phase.

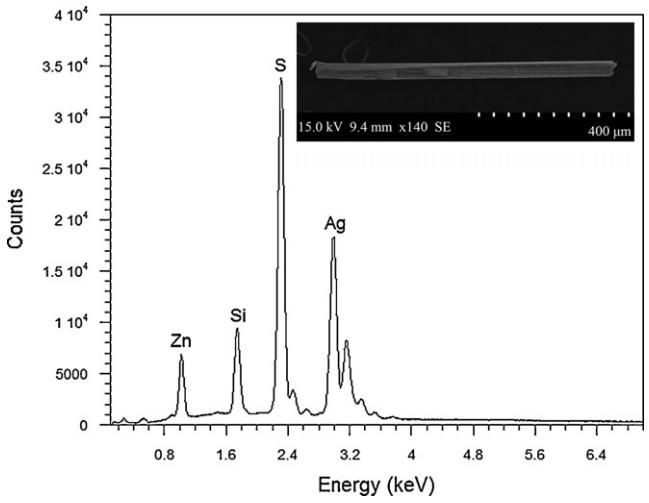

Fig. 4. Energy dispersive X-ray spectrum of Ag_2ZnSiS_4 crystal with an inlayed scanning electron micrograph of the same crystal.

3.2. Structure

Single crystal X-ray diffraction data reveal that Ag_2ZnSiS_4 crystallizes in the monoclinic noncentrosymetric space group *Pn*. All ions are tetrahedrally coordinated and reside in general positions. Each sulfur anion is surrounded by two silver cations, one zinc cation, and one silicon cation in accordance to Pauling's 2nd rule of local electroneutrality [9]. In this ordered structure the metal—sulfur bond lengths can be separated into three distinct categories. Bond distances for Ag—S show an average length of 2.539(1) Å for Ag(1) and 2.575(2) Å for Ag(2). These distances compare well to those found for the quaternary DLS compounds Ag_2HgSnS_4 with an average Ag—S bond length of 2.43(2) Å [21] and the related compound Ag_2ZnGeS_4 with an average Ag—S bond length of 2.578(5) Å [22]. The Zn—S bond has an average length of 2.344(2) Å which corresponds well with the average of 2.372(1) Å and 2.35(2) Å found in Ag_2ZnGeS_4 [22] and Li_2ZnSnS_4, respectively [23]. The distances of the Si—S bonds average 2.128(4) Å in accordance to the bond lengths found in Cu_2MnSiS_4 and Cu_2ZnSiS_4 which have averages of 2.136(1) Å [24] and 2.136(1) Å [25], respectively.

Although a less common structure type for diamond-like compounds, the *Pn* space group was first observed in these materials in 1969 by Joubert-Bettan et al. for Na_2ZnSiO_4 [26]. This wurtz–kesterite structure type was also observed in the more recent study by Lekse et al. (2008) for the compound Li_2ZnSnS_4 [23]. However, the structure of Ag_2ZnSiS_4 was not completely unexpected, due to the predictions from Chen et al. in 2010 who preformed Madelung energy calculations for different structure types on a number of known and predicted diamond-like compounds and predicted *Pc* (equivalent to *Pn*) to be the most energetically favorable for Ag_2ZnSiS_4 [27].

The structure of Ag_2ZnSiS_4 can be described as a hexagonal, closest-packed array of sulfur anions with Ag^{1+}, Zn^{2+} and Si^{4+} occupying tetrahedral holes. The structure can be viewed as a corner-sharing, three-dimensional network of MS_4 tetrahedra. When viewed down the *b*-axis one can notice (Fig. 5) the alternating nature of the cations. Rows along the *a*-axis of alternating Ag(1)-S_4 and Zn(1)-S_4 tetrahedra (ABAB) are separated by rows of Ag(2)-S_4 and Si(1)-S_4 tetrahedra (CDCD). The pattern is then alternated (BABA) and (DCDC) after which it repeats. This structure differs from the more common diamond-like wurtz–stannite structure, $Pmn2_1$ in the cation ordering. In $Pmn2_1$ there is only one unique site for the M^{1+} ions and they are aligned in rows down the *c*-axis, which is demonstrated by the comparison to the previously reported Cu_2ZnSiS_4 compound (Fig. 5) [25]. Similarly, the difference between the *Pn* and $Pna2_1$ space groups is the cation ordering for example the location of the Zn^{2+} ion with respect to the Si^{4+} site as illustrated by the comparison to Ag_2CdGeS_4 in Fig. 5 [28].

3.3. Electronic band structure and density of states (DOS)

The calculated electronic band structure of Ag_2ZnSiS_4 and $AgGaS_2$ are shown in Fig. 6(a) and (b) respectively. It is seen that for both compounds both the valence band maximum (VBMa) and the conduction band minimum (CBMi) are at the Γ-point of the BZ. These plots also show that the compounds are direct band gap semiconductors. As shown in Fig. 6(a), the Fermi level (E_F) for Ag_2ZnSiS_4 (corresponding to 0 eV energy) lies slightly above the VBMa. The difference between the CBMi and VBMa yields a band gap (E_g) of 1.88 eV for Ag_2ZnSiS_4. Whereas, in $AgGaS_2$ the Fermi level (E_F) lies slightly below the VBMa; the value of E_g in this case

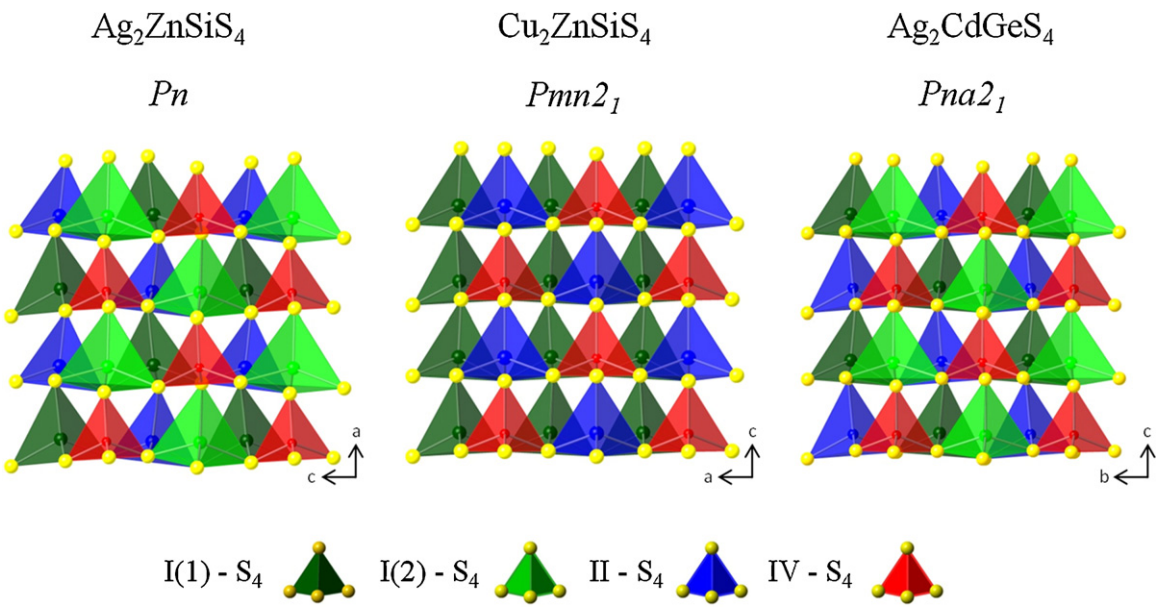

Fig. 5. Polyhedral view of Ag_2ZnSiS_4 extended to show long range cation ordering in comparison to the equivalent views of the similar compounds Cu_2ZnSiS_4 and Ag_2CdGeS_4.

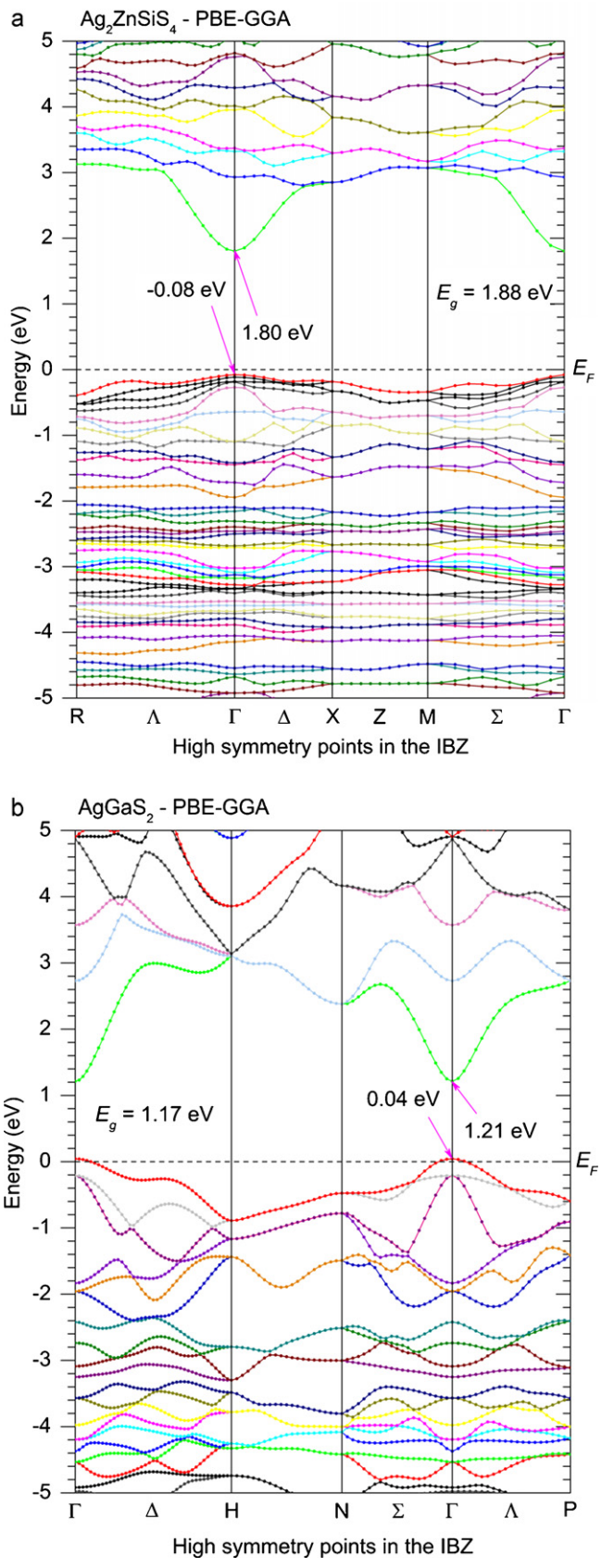

Fig. 6. Calculated electronic band structure of Ag_2ZnSiS_4 (a) is compared with that of $AgGaS_2$ (b). The graphs are scaled for 0 eV at the Fermi level (E_F).

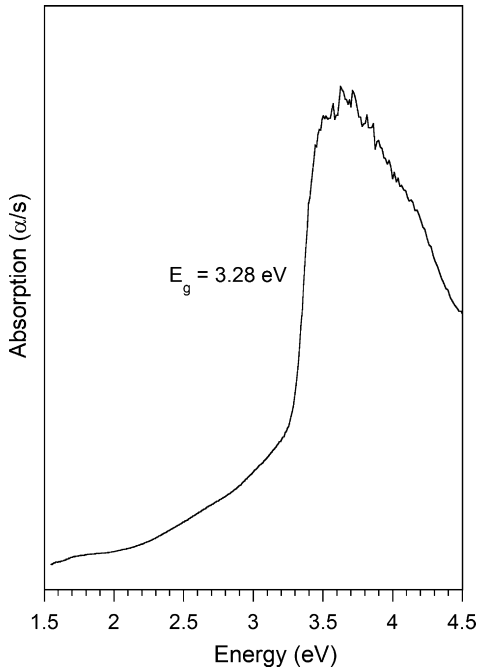

Fig. 7. Optical diffuse reflectance UV/Vis/NIR spectrum converted to absorption for Ag_2ZnSiS_4.

is 1.21 eV. The experimentally determined band gap of $AgGaS_2$ is 2.51 eV, (1.3 eV higher than our calculated value) [20,27,29]. While UV/Vis/NIR spectroscopic analysis of Ag_2ZnSiS_4 yielded an estimated band gap of 3.28 eV (Fig. 7), which is 1.4 eV higher than our calculated value.

Since the band structure of $AgGaS_2$ has been determined previously, we sought to compare our results to the previous work. Even though the same PBE-GGA has been used, the calculated E_g in the work reported here is a little higher than that which was reported by M.G. Brik (1.00 eV) using Materials Studio 4.0 package with CASTEP [20]. It is also noted that both Laksari et al. [10] and Chahed et al. [30] have reported that $AgGaS_2$ has a direct band gap of 0.95 eV both calculated using the local density approximation (LDA) in Wien2k. (In fact, our calculations using LSDA in Wien2k also yielded the same 0.95 eV band gap for $AgGaS_2$ and the details are given in Supplementary Material.) Therefore it is clear that the PBE-GGA provides a relatively better, even though underestimated, estimation of the band gap, in comparison to LDA/LSDA using the Wien2k program. It is also worth noting here that there are new exchange correlation functionals such as the Heyd–Scuseria–Ernzerhof (HSE) hybrid functional [31]. Paier et al. was able to calculate a band structure for the quaternary diamond-like semiconductor Cu_2ZnSnS_4 (CZTS), using HSE hybrid functional, that is equivalent to the measured 1.5 eV band gap of the material [31]. This functional is yet to be implemented for Wien2k; so although it underestimates the band gap, (PBE-)GGA is used in this study. Therefore the underestimation of the band gap considered in this comparison is expected.

The calculated DOS and partial DOS plots for Ag_2ZnSiS_4 and $AgGaS_2$ shown in Fig. 8(a) and (b) clearly demonstrate the semiconducting nature of these compounds. In both Ag_2ZnSiS_4 and $AgGaS_2$, the valence band (VB) close to the Fermi level has major contribution from the Ag-4d and S-3p states although there is significant, but relatively small, contribution from the 3p states of Zn and Si or the 3p and 4p states of Ga. A very weak contribution in this region from the Zn-3d states can also be seen. The hybridization of the Ag-4d states with the S-3p and the p states of other atoms in the crystal is well known as the p-d hybridization which is responsible for the red-shift of the optical band gap in these materials with

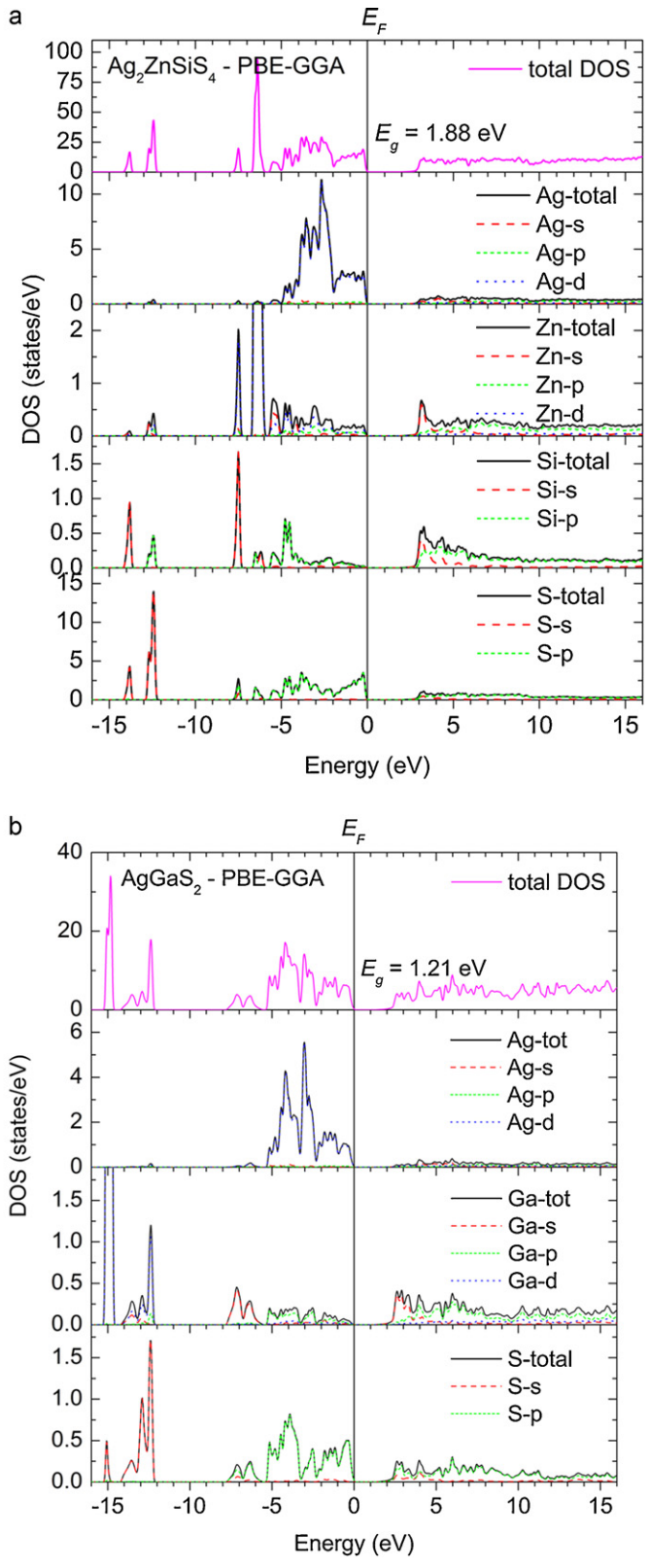

Fig. 8. Calculated total and partial density of states for Ag_2ZnSiS_4 (a) and $AgGaS_2$ (b). The graphs are scaled for 0 eV at the Fermi level (E_F).

reference to that of their binary analogs [32]. For example the binary DLSs, ZnS and GaS have an optical band gap of 3.6 and 2.5 eV respectively [33]. The states around the CBMi are mostly contributed by the Zn-4s/Ga-4s and Si-3s and 3p states. There is also a small contribution from the Zn-3p states and S-3s and 3p states, and a weak contribution from the Ag-5s and 4p states. The majority of the Zn-3d states lie deep in the VB in the energy range of −6.0 to −8.0 eV and the major contribution of Si-3s states are also deep in the valence band in the energy range of −6.0 to −8.0 eV as well as around −14.0 eV. Similarly, the major portion of Ga-3d states are in the energy range of −12 to −15.3 eV in the core of the VB. The major part of S-3s states are also in the core of the valence band in the energy range of −12.0 to −14.2 eV with considerably less contribution around −7.5 eV. Ultimately, the presence of strong p-d hybridization (more of 4d states of Ag and less of Zn/Ga) mainly constitutes the VBMa while the conduction band is mainly constituted by the mixing of s, p states and very little of the d orbitals of the atoms. The same effects of p–d hybridization have also been reported in $CuGaS_2$ [20,32].

4. Conclusion

Single crystals of the quaternary diamond-like semiconductor Ag_2ZnSiS_4 have been synthesized via high-temperature solid-state synthesis. The crystal structure was solved in the monoclinic space group *Pn*. Electronic band structure calculations show a direct energy gap of 1.88 eV, which suggests that the title compound is suitable for applications in optoelectronic devices such as LEDs [34]. Partial (or full) replacement of Zn by magnetic ions such as Cr, Mn, Fe, Co, or Ni could establish interesting magnetic properties in the material, while retaining the semiconducting and optical properties for applications in spin-based electronics [35–36]. Substitution would also help in the fine-tuning of the band gap due to the finite but small contribution of 3d-orbitals to the valence band maximum and conduction band minimum of the band structure. Since the metal (Zn) 3d states have less influence on the energy gap and are mostly confined sufficiently deep in the valence band, this system is suitable for localizing the magnetic moments while retaining the semiconducting behavior [37].

Acknowledgements

This work was supported by the National Science Foundation through a CAREER award (DMR-0645304). The powder X-ray diffractometer, the single crystal X-ray diffractometer and the scanning electron microscope were all purchased with funding from the National Science Foundation under grants DUE-0511444, CHE-0234872 and CHE-0923183.

Appendix A. Supplementary data

Supplementary data associated with this article can be found, in the online version, at doi:10.1016/j.jallcom.2011.11.133.

References

[1] X. Shi, L. Xi, J. Fan, W. Zhang, L. Chen, Chem. Mater. 22 (2010) 6029–6031.
[2] X.Y. Shi, F.Q. Huang, M.L. Liu, L.D. Chen, Appl. Phys. Lett. 94 (2009) 122103.
[3] C. Steinhagen, M.G. Panthani, V. Akhavan, B. Goodfellow, B. Koo, B.A. Korgel, J. Am. Chem. Soc. 131 (2009) 12554–12555.
[4] J.W. Lekse, M.A. Moreau, K.L. McNerny, J. Yeon, P.S. Halasyamani, J.A. Aitken, Inorg. Chem. 48 (2009) 7516–7518.
[5] W. Ruderman, J. Maffetone, D. Zelman, D. Poirier, Mater. Res. Soc. Symp. Proc. 484 (1998) 519–524.
[6] G. Catella, D. Burlage, MRS Bull. 23 (1998) 28–36.
[7] E. Parthé, Crystal Chemistry of Tetrahedral Structures, Gordon and Breach Science Publishers, New York, NY, 1964.
[8] N.A. Goryunova, in: J.C. Anderson (Ed.), The Chemistry of Diamond-like Semiconductors, The M.I.T. Press, Cambridge, 1965 (Chapters 1–3).
[9] L. Pauling, J. Am. Chem. Soc. 51 (1929) 1010–1026.
[10] S. Laksari, A. Chahed, N. Abbouni, O. Benhelal, B. Abbar, Comp. Mater. Sci. 38 (2006) 223–230.
[11] Bruker, SMART and SAINT, Bruker AXS Inc., Madison, WI, USA, 1998.
[12] G.M. Sheldrick, SADABS, University of Göttingen, Germany, 2002.
[13] Bruker, SHELXTL-PC, Release 6.14, Bruker AXS Inc., Madison, WI, USA, 2007.

[14] D. Palmer, Crystal Maker, CrystalMaker Software Ltd., Oxfordshire, England, 2010.
[15] X.P.H. Plus, PANalytical B.V., (2006). Almelo, the Netherlands.
[16] P. Kubelka, F. Munk, Zeit. Für Tekn. Physik 12 (1931) 593.
[17] K. Schwarz, P. Blaha, G.K.H. Madsen, Comp. Phys. Commun. 147 (2002) 71–76.
[18] K. Schwarz, J. Solid State Chem. 176 (2003) 319–328.
[19] P. Blaha, K. Schwarz, G.K.H. Madsen, D. Kvasnicka, J. Luitz, Vienna University of Technology, Austria (2011) ISBN 3-9501031-1-2.
[20] M.G. Brik, J. Phys.: Condens. Matter 21 (2009) 485502.
[21] O.V. Parasyuk, S.I. Chykhrij, V.V. Bozhko, L.V. Piskach, M.S. Bogdanyuk, I.D. Olekseyuk, L.V. Bulatetska, V.I. Pekhnyo, J. Alloys Compd. 399 (2005) 32–37.
[22] O.V. Parasyuk, A.O. Fedorchuk, Yu.M. Kogut, L.V. Piskach, I.D. Olekseyuk, J. Alloys Compd. 500 (2010) 26–29.
[23] J.W. Lekse, B.M. Leverett, C.H. Lake, J.A. Aitken, J. Solid State Chem. 181 (2008) 3217–3222.
[24] T. Bernert, A. Pfitzner, Z. Kristallogr. 220 (2005) 968–972.
[25] K.A. Rosmus, J.A. Aitken, Acta Cryst. E 67 (2011) i28.
[26] C.A. Joubert-Bettan, R. Lachenal, E.F. Bertraut, E. Parthè, J. Solid State Chem. 1 (1969) 1–5.
[27] S. Chen, A. Walsh, Y. Luo, J.H. Yang, X.G. Gong, S.H. Wei, Phys. Rev. B 82 (2010) 95203.
[28] C.D. Brunetta, W.C. Minsterman III, C.H. Lake, J.A. Aitken, J. Solid State Chem., (under revision).
[29] W.N. Honeyman, K.H. Wilkinson, J. Phys. D: Appl. Phys. 4 (1971) 1182.
[30] A. Chahed, O. Benhelal, S. Laksari, B. Abbar, B. Bouhafs, N. Amrane, Physica B 367 (2005) 142–151.
[31] J. Paier, R. Asahi, A. Nagoya, G. Kresse, Phys. Rev. B 79 (2009) 115126.
[32] J.L. Shay, B. Tell, H.M. Kasper, L.M. Schiavone, Phys. Rev. B 5 (1972) 5003.
[33] O. Madelung, M. Schulz (Eds.), Numerical Data and Functional Relationships in Science and Technology. New Series. Group III: Crystal and Solid State Physics. Semiconductors. Supplements and Extensions to Volume III/17. Intrinsic Properties of Group IV Elements and III–V, II–VI and I–VII Compounds, vol. 22a, Springer, Berlin, 1982.
[34] J.L. Shay, B. Tell, H.M. Kasper, Appl. Phys. Lett. 19 (1971) 366.
[35] S.J. Pearton, C.R. Abernathy, D.P. Norton, A.F. Hebard, Y.D. Park, L.A. Boatner, J.D. Budai, Mater. Sci. Eng., R 40 (2003) 137–168.
[36] S.A. Wolf, D.D. Awschalom, R.A. Buhrman, J.M. Daughton, S. von Molnár, M.L. Roukes, A.Y. Chtchelkanova, D.M. Treger, Science 294 (2001) 1488–1495.
[37] K. Sato, L. Bergqvist, J. Kudrnovský, P.H. Dederichs, O. Eriksson, I. Turek, B. Sanyal, G. Bouzerar, H. Katayama-Yoshida, V.A. Dinh, T. Fukushima, H. Kizaki, R. Zeller, Rev. Mod. Phys. 82 (2010) 1633.